

Ultraviolet photodissociation of the HCCO radical studied by fast radical beam photofragment translational spectroscopy

David H. Mordant, David L. Osborn, Hyeon Choi, Ryan T. Bise, and Daniel M. Neumark
Department of Chemistry, University of California, Berkeley, California 94720
and Chemical Sciences Division, Lawrence Berkeley National Laboratory, Berkeley, California 94720

(Received 16 May 1996; accepted 7 August 1996)

The ultraviolet photolysis of jet-cooled mass-selected ketyl radicals has been investigated using the technique of fast radical beam photofragment translational spectroscopy. The $\tilde{C}^2\Pi(^2A'')$ – \tilde{X}^2A'' photofragment yield cross section spans 33 400–48 000 cm^{-1} and exhibits resolved resonances and broad continua. Dissociation produces both ground and excited state CH radicals in association with ground state CO fragments; there is no evidence for H atom elimination. Analysis of the photofragment kinetic energy release spectra yield a value for the C–C bond dissociation energy and heat of formation of HCCO: $D_0(\text{HC–CO})=3.14\pm 0.03$ eV (72.4 ± 0.7 kcal/mol) and $\Delta H_{f,0}^0(\text{HCCO})=1.82\pm 0.03$ eV (42.0 ± 0.7 kcal/mol). © 1996 American Institute of Physics.
[S0021-9606(96)03938-4]

The ketyl (HCCO) free radical is a short lived combustion intermediate of acetylene and larger unsaturated hydrocarbons.¹ The majority (ca. 80%) of acetylene molecules are oxidized via the HCCO intermediate.^{2–4} A major obstacle to the study of acetylene combustion has been the previous lack of a sensitive visible-ultraviolet (UV) spectroscopic probe for the HCCO species. The mechanism for acetylene oxidation is still unresolved.

Despite its importance, the HCCO radical has received only minor experimental attention. Oakes *et al.*⁵ measured the photoelectron spectrum of the HCCO^- anion, yielding the electron affinity and heat of formation of HCCO. The microwave rotational spectrum^{6,7} of HCCO was observed around 21 GHz and from 325–390 GHz and showed the ground state geometry to be planar and quasilinear. The local C–O stretching vibrational mode was characterized in infrared absorption.^{8,9} There have been two reports^{10,11} of UV absorption bands centered around $\nu=28\,500$ cm^{-1} , but neither is definitive. The latter has since been determined to be entirely due to formaldehyde molecules.¹² Electronic structure calculations^{13–18} predict the energy, minimum energy configuration, and fundamental vibrational frequencies of the \tilde{X}^2A'' , $\tilde{A}^2\Pi(^2A')$, \tilde{a}^4A'' , \tilde{B}^2A' , and $\tilde{C}^2\Pi(^2A'')$ electronic states.

In this communication, the first observation of an electronic transition for the HCCO radical is presented. For this electronic band, we report the UV photofragment yield cross section, the photoproducts, and total kinetic energy release spectra as a function of energy. These observations allow us to identify the potential energy surfaces involved in electronic excitation and dissociation, and to refine the HC–CO bond dissociation energy.

The photodissociation of HCCO radicals is studied using fast radical beam photofragment translational spectroscopy. A full description of the technique has been previously reported.^{19–21} In brief, HCCO^- ions are formed by an electrical discharge²² in a pulsed supersonic expansion of $\text{HCCH:N}_2\text{O:O}_2\text{:Ne}$ (with a mixing ratio of 1:3:6:90, respec-

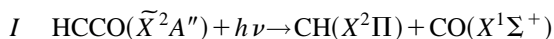
tively) using a backing pressure of 45 psi. The ions are accelerated to 8000 eV and mass selected by time-of-flight. The HCCO^- ions are selectively photodetached at threshold⁵ with a pulsed dye laser tuned to 19 225 cm^{-1} . The result is a fast, isentropically cooled, mass-selected beam of HCCO radicals.

The resultant neutral HCCO radicals are intersected by a pulsed UV photolysis laser beam, resulting in photofragments with high laboratory kinetic energy. These can be detected very efficiently with a microchannel plate detector. Two types of experiment are performed.

A. The photolysis frequency is scanned and the total flux of photofragments is detected, providing the photofragment yield cross section as a function of frequency.

B. At selected photolysis energies, the photofragments are collected *in coincidence* using a universal time- and position-sensitive detector. This yields the kinetic energy release, scattering angle, and photofragment masses for each dissociation event.

Figure 1 reports the photofragment yield cross section from 32 500–48 000 cm^{-1} . The apparent vibrational band origin is located at 33 403 cm^{-1} ; reproducible vibrational structure is observed up to 38 000 cm^{-1} . Higher resolution scans reveal resolved *rotational* structure for several vibrational bands near the origin, an example is given in the inset in Fig. 1. As the excitation energy is increased the resonances broaden; rotational structure cannot be resolved above 35 000 cm^{-1} , and individual vibrational resonances cannot be resolved above 38 000 cm^{-1} . Based on literature heats of formation,^{5,23–25} three dissociation pathways are accessible to HCCO at the excitation energies in Fig. 1:



$$\Delta_r H_0 = 3.14 \pm 0.03 \text{ eV}, \quad (3.12 \text{ eV})$$

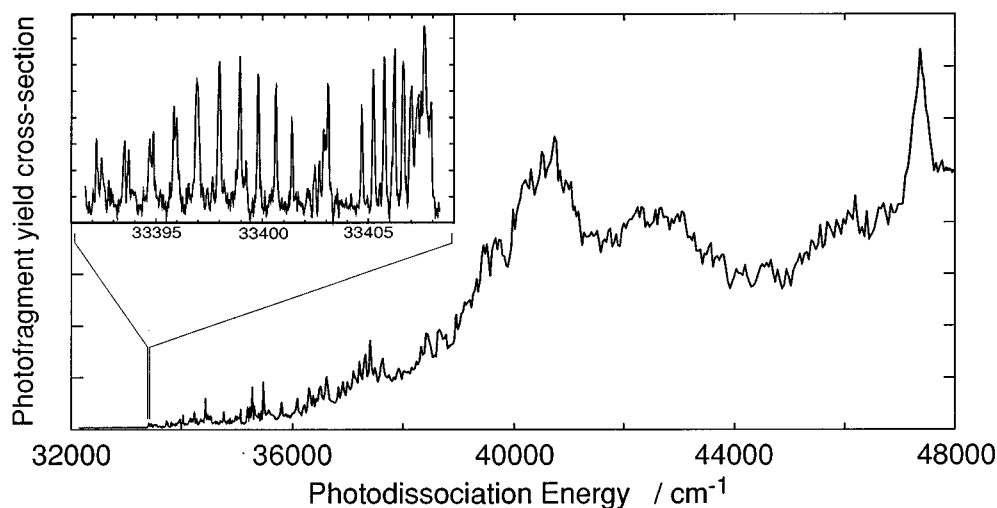
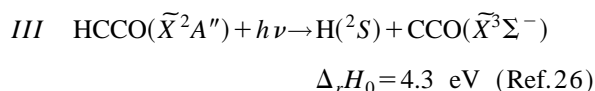
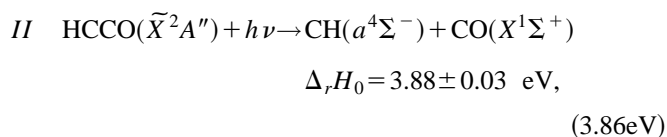


FIG. 1. Ultraviolet photofragment yield cross section for the $\tilde{C}^2\Pi(^2A'')-\tilde{X}^2A''$ electronic transition in the HCCO radical. The insert identifies rotationally-resolved resonances at the band origin.



with $\Delta_r H_0$ defining the enthalpy of the reaction at 0 K. The values for channels *I* and *II* with quoted errors are based on this work; those in parentheses are the previous literature values.

Figure 2 shows photofragment translational energy dis-

tributions, $P(E_T)$, for the CH+CO mass channel (i.e., channels *I* and *II*) at six excitation energies, obtained using the coincidence detection scheme mentioned above. The maximum kinetic energies for channels *I* and *II* are indicated on all six spectra. The coincidence method cannot be used to detect the H+CCO channel, because the fragment masses are too disparate. However, a noncoincident photofragment time-of-flight scheme,²⁷ shows no evidence of H atom elimination for HCCO, channel *III*. Therefore, within the limits of our experiment, dissociation from the electronic band in Fig. 1 results solely in CH+CO production.

The $P(E_T)$ distributions for the four lowest excitation

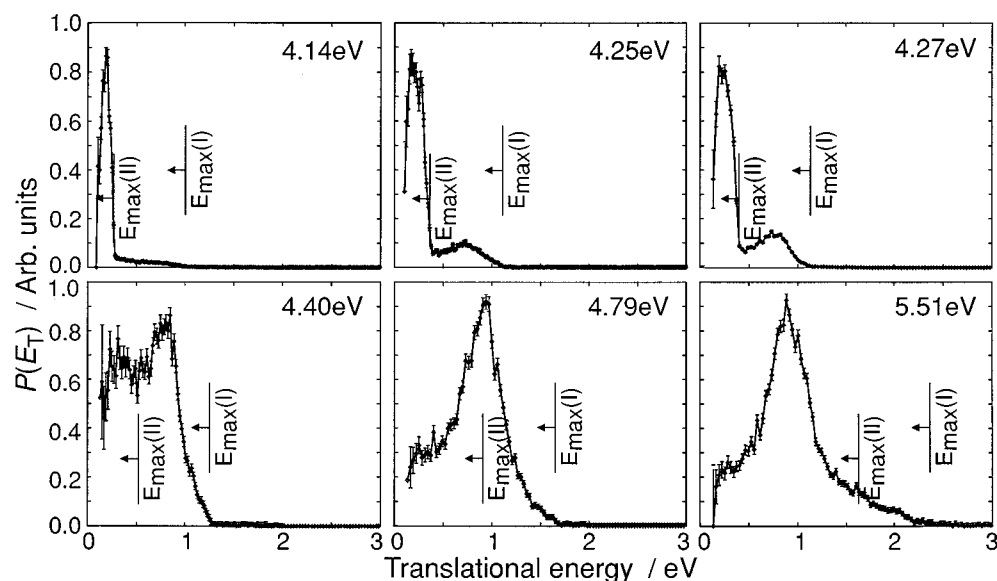


FIG. 2. Photofragment translational energy distributions, $P(E_T)$, resulting from the UV dissociation of the HCCO radical at six excitation energies. Using a bond dissociation energy of $D_0(\text{HC}-\text{CO})=3.14 \pm 0.03 \text{ eV}$, $E_{\text{max}}(\text{I})$ and $E_{\text{max}}(\text{II})$ indicate the maximum kinetic energy threshold for the production of: (I) CH($X^2\Pi$)+CO($X^1\Sigma^+$) and (II) CH($a^4\Sigma^-$)+CO($X^1\Sigma^+$) photofragments, respectively.

energies each consist of two distinct peaks. From the energetic thresholds given above, the onset of the lower energy peak corresponds to the maximum kinetic energy release allowed for channel *II*, $\text{CH}(a^4\Sigma^-) + \text{CO}$, while that for the higher energy feature corresponds to channel *I*, $\text{CH}(X^2\Pi) + \text{CO}$. The relative intensity of the peak at higher kinetic energy rises abruptly across the small excitation energy range (0.26 eV) spanned by the four spectra. Channel *II*, therefore, dominates at the lowest excitation energies, while the contribution from channel *I* rapidly increases with excitation energy. Note that this is the energy range over which rotationally-resolved resonances occur in the photodissociation cross section, indicating a slow dissociation rate.

In spite of the large difference (0.72 eV) in excitation energy, the $P(E_T)$ distributions at 4.79 and 5.51 eV are similar in form, consisting of a single peak with a maximum intensity at 0.9 eV, and a high energy tail that extends to the maximum allowed translational energy for channel *I*. The peak at 0.9 eV is very close to the maximum of the higher energy peak assigned to channel *I* in the spectra at 4.25, 4.27, and 4.40 eV. By analogy, we assign this peak to channel *I* in the two higher energy spectra as well. Based on this, we attribute the majority of the products at these two energies to channel *I*.

The coincidence measurements also yield photofragment angular distributions. The photofragment recoil anisotropy parameters, $\beta(E)$, for all investigated photolysis energies are positive. These values are independent of channel *I* or *II* products, although there is a small degree of variation with total kinetic energy. The average value of $\beta(E)$ is 0.7 ± 0.1 .

As this is the first observation of an electronic transition for the HCCO radical, the electronic states involved must be identified. HCCO has a \tilde{X}^2A'' ground state.^{6,7} The bent \tilde{B}^2A' and linear $\tilde{C}^2\Pi(2A'')$ electronic states are predicted¹⁷ to be located in the energy regime of the spectrum in Fig. 1. Since all the photofragment recoil anisotropy parameters are positive we deduce that the observed cross section is due to a single parallel electronic transition. In addition, the rotational structure in the cross section suggests that the upper electronic state is linear.²⁸ Hence, we assign the spectrum in Fig. 1 to the parallel $\tilde{C}^2\Pi(2A'')$ – \tilde{X}^2A'' optical transition.

Consideration of spin conservation and symmetry shows that the $\tilde{C}^2\Pi(2A'')$ state correlates with highly excited products. Channel *I* products correlate with the \tilde{X}^2A'' and $\tilde{A}^2\Pi(2A')$ electronic states of HCCO, whereas channel *II* products only correlate with the \tilde{a}^4A'' state (see Fig. 3).

Our results show that at least two competing dissociation mechanisms are present; this can be interpreted with the aid of Fig. 3. Near the band origin, dissociation occurs almost entirely to the higher energy, spin-forbidden $\text{CH}(a^4\Sigma^-) + \text{CO}(X^1\Sigma^+)$ channel. This mechanism presumably involves intersystem crossing (ISC) from the $\tilde{C}^2\Pi(2A'')$ state to the low-lying \tilde{a}^4A'' state. The dissociation cross section at the band origin is highly structured; the linewidths of the rotationally-resolved resonances are limited by the laser

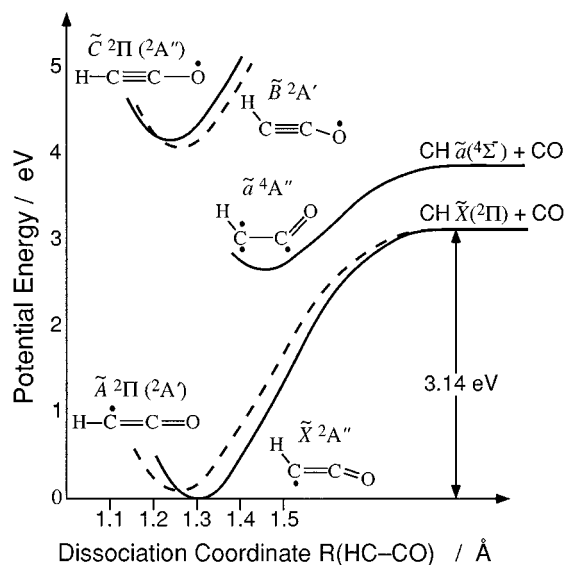


FIG. 3. Schematic adiabatic curves for the \tilde{X}^2A'' , $\tilde{A}^2\Pi(2A')$, \tilde{a}^4A'' , \tilde{B}^2A' , and $\tilde{C}^2\Pi(2A'')$ electronic states of the HCCO radical, illustrating the product correlation with ground and excited state $\text{CH} + \text{CO}$ fragments. The \tilde{C} – \tilde{X} spacing (4.14 eV) and the C–C bond dissociation energy (3.14 eV) are obtained from our present work. The \tilde{a} – \tilde{X} spacing (2.35 eV) is obtained from Hu *et al.* (Ref. 18) and the difference between doublet and quartet states in CH is 0.74 eV (Ref. 24). Minimum energy configurations are obtained from Kim and Shavitt (Ref. 17) and Hu *et al.* (Ref. 18).

resolution (0.1 cm^{-1}), reflecting the slow ISC rate. At higher excitation energies, channel *I* is the major dissociation pathway, and the cross section is unstructured. This suggests that predissociation occurs by fast internal conversion (IC) to high vibrational levels on the \tilde{X}^2A'' state leading to spin-allowed $\text{CH}(X^2\Pi) + \text{CO}(X^1\Sigma^+)$ products. The increased contribution of IC at higher excitation energies may simply be due to the higher vibrational level density of the \tilde{X}^2A'' state, or it may be due to a curve-crossing between the \tilde{X} and \tilde{C} states; these and other aspects of the dissociation dynamics will be considered in an upcoming publication.²⁸

Finally, the onsets of the peaks corresponding to channel *II* for the three lowest excitation energies directly yield $\Delta_f H_0 = 3.88 \pm 0.03 \text{ eV}$ for this channel. Combining this with the $a^4\Sigma^-$ – $X^2\Pi$ splitting in CH^{24} and heats of formation of CH and CO^{23} yields both the bond dissociation energy and heat of formation for HCCO: $D_0(\text{HC-CO}) = 3.14 \pm 0.03 \text{ eV}$ ($72.4 \pm 0.7 \text{ kcal/mol}$) and $\Delta H_{f,0}^0(\text{HCCO}) = 1.82 \pm 0.03 \text{ eV}$ ($42.0 \pm 0.7 \text{ kcal/mol}$). The latter value supports and further refines the currently accepted value^{5,23} of $1.84 \pm 0.09 \text{ eV}$ and corrects a previous determination²⁹ of the heat of formation.

In summary, the electronic spectroscopy and photodissociation dynamics of the HCCO radical exhibit rather unusual features. The $\tilde{C}^2\Pi(2A'')$ – \tilde{X}^2A'' evolves from a rotationally-resolved spectrum near the origin to an unstructured spectrum at only slightly higher excitation energies. The dynamics results show that dissociation to the higher energy, spin-forbidden $\text{CH}(a^4\Sigma^-) + \text{CO}$ channel dominates at low excitation energy, and the lower energy but spin-allowed

CH($X^2\Pi$)+CO product becomes the major channel at higher excitation energies. The disappearance of structure in the spectrum is clearly correlated with the appearance of the spin-allowed channel, but the apparent suppression of this channel near the band origin is intriguing and requires a better understanding of the HCCO potential energy surfaces and their interactions.

This research is supported by the Director, Office of Energy Research, Office of Basic Energy Sciences, Chemical Sciences Division of the U.S. Department of Energy under Contract No. DE-AC03-76SF00098. The authors thank Dr. Celeste Rohlffing and Professor Ian Smith for helpful discussions. D.H.M. is a NATO science research fellow. D.M.N. is a Camille and Henry Dreyfus Teacher-Scholar.

¹I. T. N. Jones and K. D. Bayes, *J. Am. Chem. Soc.* **94**, 6869 (1972).

²J. V. Michael and A. F. Wagner, *J. Phys. Chem.* **94**, 2453 (1990).

³W. Bouilart and J. Peeters, *J. Phys. Chem.* **96**, 9810 (1992).

⁴J. Peeters, I. Langhans, and W. Bouilart, *Int. J. Chem. Kinet.* **26**, 869 (1994).

⁵J. M. Oakes *et al.*, *J. Phys. Chem.* **87**, 4810 (1983).

⁶Y. Ohshima and Y. Endo, *J. Mol. Spec.* **159**, 458 (1993).

⁷Y. Endo and E. Hirota, *J. Chem. Phys.* **86**, 4319 (1987).

⁸K. G. Unfried, G. P. Glass, and R. F. Curl, *Chem. Phys. Lett.* **177**, 33 (1991).

⁹M. Jacox and B. Olson, *J. Chem. Phys.* **86**, 3134 (1987).

¹⁰S. L. N. G. Krishnamachari and R. Venkatasubramanian, *Pramana* **23**, 321 (1984).

¹¹G. Inoue and M. Suzuki, *J. Chem. Phys.* **84**, 3709 (1986).

¹²M. A. Hanratty and H. H. Nelson, *J. Chem. Phys.* **92**, 814 (1990).

¹³L. B. Harding, *J. Phys. Chem.* **85**, 10 (1981).

¹⁴J. D. Goddard, *Chem. Phys. Lett.* **154**, 387 (1989).

¹⁵M. T. Nguyen, W. Bouilart, and J. Peeters, *J. Chem. Phys.* **98**, 8030 (1994).

¹⁶P. J. Szalay, J. F. Stanton, and R. J. Bartlett, *Chem. Phys. Lett.* **193**, 573 (1992).

¹⁷K. Kim and I. Shavitt (in preparation).

¹⁸C.-H. Hu *et al.*, *J. Am. Chem. Soc.* **115**, 6904 (1993).

¹⁹R. E. Continetti *et al.*, *Chem. Phys. Lett.* **182**, 406 (1991).

²⁰D. R. Cyr *et al.*, *J. Chem. Phys.* **97**, 4937 (1992).

²¹R. E. Continetti *et al.*, *J. Chem. Phys.* **99**, 2616 (1993).

²²D. L. Osborn *et al.*, *J. Chem. Phys.* **104**, 5026 (1996).

²³S. G. Lias *et al.*, *J. Chem. Phys. Ref. Data* **17**, Suppl. No. 1 (1988).

²⁴A. Kasdan, E. Herbst, and W. C. Lineberger, *Chem. Phys. Lett.* **31**, 78 (1975).

²⁵J. M. Van Doren *et al.*, *J. Am. Chem. Soc.* **115**, 7407 (1993).

²⁶This value is based on a recent photoelectron spectrum of CCO [V. Zenggin, B. Joakim Persson, K. M. Strong, and R. E. Continetti, *J. Chem. Phys.* (submitted)] which indicates that the value $\Delta H_{f,0}^0(\text{CCO})$ in Ref. 5 should be reduced by over 0.4 eV, placing $\Delta_r H_0$ for channel III ca. 4.3 eV.

²⁷D. L. Osborn, H. Choi, and D. M. Neumark, *Adv. Chem. Phys.* (in press).

²⁸D. L. Osborn, D. H. Mordaunt, H. Choi, R. T. Bise, and D. M. Neumark (in preparation).

²⁹J. L. Holmes and F. P. Lossing, *Int. J. Mass. Spectrom. Ion Process.* **58**, 113 (1984).